



# Trails of solar system minor bodies on WFC/ACS images <sup>☆</sup>

Simone Marchi, Yazan Momany, Luigi R. Bedin <sup>\*</sup>

*Dipartimento di Astronomia, Università di Padova, Vicolo dell'Osservatorio 2, I-35122 Padova, Italy*

Received 7 May 2004; received in revised form 18 June 2004; accepted 6 July 2004

Available online 7 August 2004

Communicated by F.D. Macchetto

---

## Abstract

In this paper, we analyse very short arcs of minor bodies of the Solar System detected on Hubble Space Telescope (*HST*) Wide Field Channel ACS images. In particular, we address how to constrain the Keplerian orbital elements for minor body detections, illustrating the method for two objects. One of the minor bodies left 13 successive trails, making it the most well-sampled object yet identified in the *HST* archive. Most interestingly, we also address the problem of ephemeris prediction and show that in the particular case of *HST* very short arcs the confinement window for subsequent recovery is *significantly reduced to a narrow linear region*, that would facilitate successive observations.

© 2004 Elsevier B.V. All rights reserved.

PACS: 96.30.Y

Keywords: Minor planets

---

## 1. Introduction

Although the *HST* was not specifically designed to serve as an asteroid surveyor, it offers a unique

opportunity to study the solar system minor objects (MOs). Indeed, MO trails on the *HST* images are usually characterized by a curved shape, whereas in ground-based observations they will stand out only as straight lines (for typical exposure times). The curvature in *HST* images is simply due to the parallax induced by the telescope orbital motion while exposing, and is easily detectable owing to its high angular resolution. Taking into account the specific observation conditions (i.e., the ephemeris of the *HST* while exposing), it is possible to simulate trails as a function of geocentric distance and line of sight. Thus, a comparison of

---

<sup>☆</sup> Based on observations with the NASA/ESA *Hubble Space Telescope* (GO9820), obtained at the Space Telescope Science Institute, which is operated by AURA, Inc., under NASA contract NAS 5-26555.

<sup>\*</sup> Corresponding author. Tel.: +39 049 827 82; fax: +39 049 827 8212.

E-mail addresses: [marchi@pd.astro.it](mailto:marchi@pd.astro.it) (S. Marchi), [momany@pd.astro.it](mailto:momany@pd.astro.it) (Y. Momany), [bedin@pd.astro.it](mailto:bedin@pd.astro.it) (L.R. Bedin).

the observed trail with the simulated ones, enables a distance determination of the detected MOs.

This method has been illustrated in the work of Evans et al. (1998), which presented trails of 96 MOs, detected on 28,460 WFPC2 deep *HST* images. Most of these MOs are too faint to have been detected in ground-based observations. In this regard, the recent advent of the Advanced Camera for Surveys (ACS) offers new perspectives. Indeed, the Wide Field Channel (WFC) of the ACS has a smaller pixel scale than the wide field cameras of WFPC2; it is up to  $\sim 5$  times more sensitive; and most interestingly, it offers a field of view which is two times wider. These aspects are of significant impact in a better tracking of the trails, lowering the limit of detectable objects; and increasing the probability of serendipitous capture of MOs within the WFC/ACS field of view. Extrapolating from the Evans et al. (1998) results, one finds that, on average, one in every 30 ACS deep exposures may unveil the trail of a new faint MO.

Once a MO has been detected, the next step would be the determination of an orbital solution, in order to calculate accurate ephemeris. The knowledge of these two is indispensable for any further investigation. The problem of MOs orbital determination has been widely discussed in the literature. Well-defined orbital solutions require several observations spanning periods of time long enough to show the curvature of their motion. However, in most cases the observed arcs are too short to obtain convergent solutions (the so-called very short arcs, VSAs, see Milani et al., 2004). In general, MO detections originate from: (1) automated surveys, e.g., LONEOS or LINEAR; (2) casually detected objects, e.g., observations obtained for other scientific purposes (as in our case), or (3) digital archive surveys, e.g., Barbieri et al. (2004). In all these cases, determinations of orbital solutions and geocentric distances from VSAs are not possible.

In this paper, we deal with a particular kind of VSAs, namely those detected with the Hubble Space Telescope (HVSAs). HVSAs can be considered an intermediate case between ground-based VSAs and detections for which full orbital solutions are determined. The main difference derives

from the fact that for HVSAs one can determine geocentric distances even if the arcs are very short (e.g., 1–2 h or less). This has a considerable impact on constraining the orbital solutions. Although a unique solution is still out of reach, useful information concerning the real nature of the detection can be obtained. Moreover, the knowledge of geocentric distances is vital in recovering these objects in successive observations. We discuss these topics by providing two examples of MOs detected on *HST*/ACS images.

## 2. Observations and data reduction

The *HST*/ACS data come from GO-9820 (P.I.: Momany), aimed at the study of the star formation history of the Local Group Sagittarius dwarf irregular galaxy (SagDIG). The central pointing of all images were centered at: ( $\alpha = 19:29:58.97$ ,  $\delta = -17:40:41.3$ ), whose ecliptic coordinates are:  $\lambda = 291.437^\circ$  and  $\beta = +4.103^\circ$  at J2000 equinox. The observations consist of a total number of three *HST* orbits, one orbit per filter and 5 exposures per orbit:  $5 \times 396$ s in F606W ( $V_{606}$ ),  $5 \times 419$ s in F475W ( $B_{475}$ ), and  $5 \times 419$ s in F814W ( $I_{814}$ ), conducted on August 18th 2003, covering a total time interval of  $\sim 3.9$  h. These images were preprocessed with the standard STScI pipeline. A correction of the geometrical distortion has been applied following the Anderson (2002) recipe.

## 3. The two MOs

### 3.1. Identification

A rapid check for passing MOs has been done by eye inspection of all available images. Using a selected sample of common stars, all single images were put onto a common reference system. The image combination was simply a sum, i.e., all particular features like cosmic rays or transiting MOs were preserved. Although this method resulted in a sum image that is full of cosmic rays, on the other hand, trails of transiting MOs stood-out as these formed a sequence of multiple trails, that were easily detected. This method helped to identify two

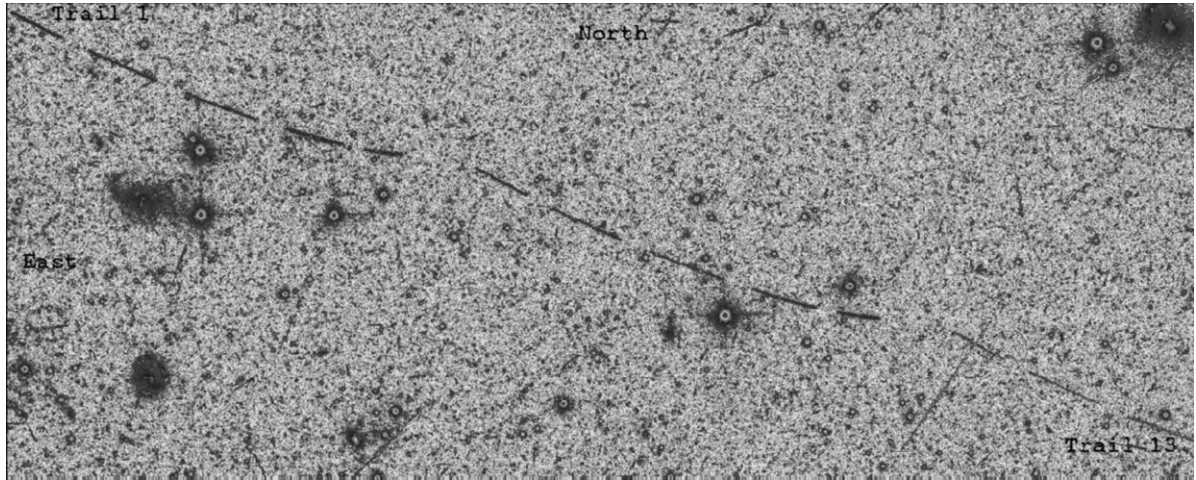


Fig. 1. The 13 trails left by MO1 on the sum image. North is up, East is to the left. The first trail is the upper left one: MO1 at  $\alpha = 19:29:56.602$  and  $\delta = -17:40:00.01$ . The last trail is the lower right one, having crossed  $\Delta\alpha = -65.1$ ,  $\Delta\delta = -25.43$  arcsec. The first 5 trails are in  $V_{606}$  filter, followed by 5 trails in  $B_{475}$  and 3 trails in  $I_{814}$ .

MOs with multiple trails. Prior to this study, the two MOs were not registered in the Minor Planet Center (MPC) (<http://scully.harvard.edu/~cgi/CheckMP>) database. The brighter one (MO1 hereafter), left 13 consecutive curved-trails covering three *HST* orbits (5 trails in the  $V_{606}$  and  $B_{475}$  filters and three trails in the  $I_{814}$  filter). The second object (MO2) left only three trails, all of them in the  $V_{606}$  filter. Fig. 1 shows the 13 trails of MO1 on the sum image. It is by far the most well-sampled asteroid trail yet identified in the *HST* archive data. MOs with even one trail can still be distinguished from cosmic rays, as MOs will reflect the telescope point spread function. We however could not identify additional objects.

### 3.2. Distances and orbits

Our analysis of individual trails follows the guidelines of the work of Evans et al. (1998). In general, the apparent motion of a minor body in the sky is due to the superposition of the observer's motion and the intrinsic motion of the object. For objects identified in *HST* images, the apparent motion  $\vec{P}$  can be written as:

$$\vec{P}(t) = \vec{P}_H(t) + \vec{P}_E(t) + \vec{P}_{MO}(t),$$

where  $\vec{P}_H$ ,  $\vec{P}_E$ ,  $\vec{P}_{MO}$  are the parallaxes due to *HST*, the Earth, and the intrinsic minor body motion,

respectively. By knowing  $\vec{P}_H$ ,  $\vec{P}_E$ , and measuring  $\vec{P}$  on the images, one can determine the intrinsic motion rate of the minor body as follows:

$$\vec{P}_{MO}(t, d(t)) = \vec{P}(t) - \vec{P}_E(t, d(t)) - \vec{P}_H(t, d(t)),$$

where we have now explicitly indicated the dependence of  $\vec{P}_H$ ,  $\vec{P}_E$ , and hence of  $\vec{P}_{MO}$ , on the MOs geocentric distance  $d$ , which also varies with time. The intrinsic rate of the minor body does change with time. However, on short timescales ( $\sim 2$ – $3$  h), we assume that it has a linear dependence with time, i.e.,  $\vec{P}_{MO}(t, d(t)) = \vec{P}_{MO}(d) \times t$ , and that  $d$  is constant. So, for each value of  $d$  we compute the corresponding  $\vec{P}_{MO}$  using the maximum time interval available, i.e., endpoints of the whole exposure sequence in the same filter. This allows us to reconstruct the trajectory of the body, for any value of  $d$  and at any given time. On the other hand, the best value of  $d$  is determined by minimizing the root mean square differences between the start/end points of the *observed* trails and *simulated* trajectories (see Fig. 2). For this task, only the start/end points of *each* trail were used, as these are the only points with time tags. Although, the actual shape of each trail has not been used in the fitting procedure [in this aspect our analysis differs from that of Evans et al. (1998)], it remains that our best estimate of  $d$  reproduces the shape of *all observed trails*. The

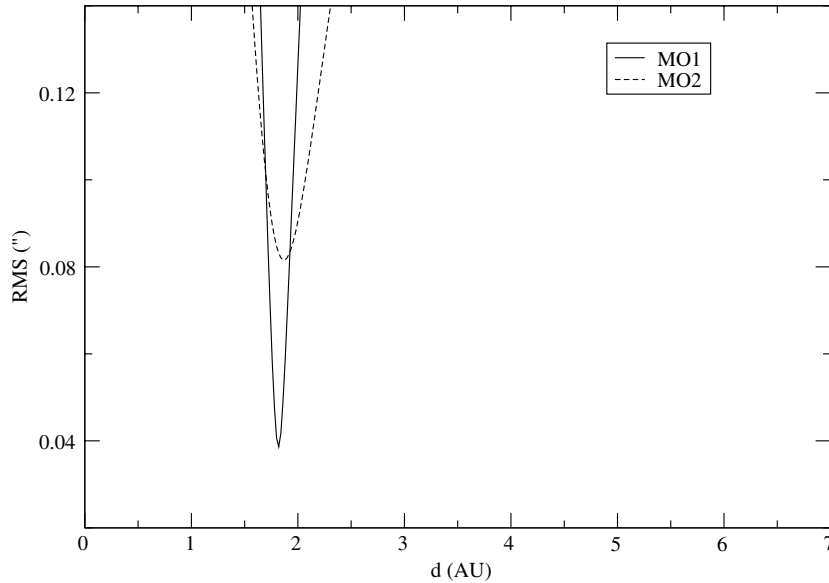


Fig. 2. Root mean square (RMS) differences (in arcsec) between the start/end points of the observed trails and simulated trajectories (see text).

resulting geocentric (heliocentric) distance for MO1 and MO2 are  $d = 1.82(2.72) \pm 0.10$  AU and  $d = 1.86(2.76) \pm 0.15$  AU, respectively. The larger error for MO2 is due to the smaller number of measured points.

Once the geocentric distance of the minor body is determined, one can compute its geocentric velocity in the plane perpendicular to the line of sight. However, the velocity component along the line of sight,  $\dot{d}$ , cannot be determined. For this reason, it is impossible to obtain a single orbital solution, as it would require the knowledge of  $d$  and  $\dot{d}$ . However, it is possible to put some constraints on the orbital elements. In order to have a bound solution, the heliocentric velocity has to be such that the total energy,  $\mathcal{E}(d, \dot{d})$ , is  $< 0$ . Hence, for each value of  $d$  for which  $\mathcal{E}(d, \dot{d}) < 0$  is satisfied, a corresponding orbital solution is obtained. The eccentricity in these solutions can vary from 0 to 1, leading to a large variation of  $a$  values. In Figs. 3 and 4, the Keplerian elements  $a$ ,  $e$ ,  $i$  for the possible solutions are plotted. It is seen that while the solutions for  $a$  and  $e$  are not well determined, the inclination instead is restricted to a narrow region. Figs. 3 and 4 also show double solutions for each value of  $a$ , corresponding to solutions with  $\dot{d}$  being

positive or negative. On the same plots, numbered asteroids (NAs) and numbered comets (NCs) distributions are shown for comparison. Judging the range of possible values for  $a$ ,  $e$  and  $i$ , it is most likely that our two MOs are main belt asteroids, although other solutions cannot be ruled out.

### 3.3. HVSA ephemeris

Although the observed arcs are very short, thanks to the fact that we are dealing with HVSA the possible orbital solutions have been significantly constrained. We now examine whether another important aspect of MO detections can be constrained, that is the recovery of these objects in successive observations. The problem of generating ephemeris for VSAs detected by ground-based telescopes has been discussed already by Milani et al. (2004). The main result of their analysis is the production of “triangulated ephemeris”, i.e., ephemeris computed on a grid of orbital solutions which sample in a proper way the VSA admissible region in the plane  $(d, \dot{d})$ . This ephemeris production for each point of the grid results in a two-dimensional portion of the sky where the MO has to be confined. The size of this confine-

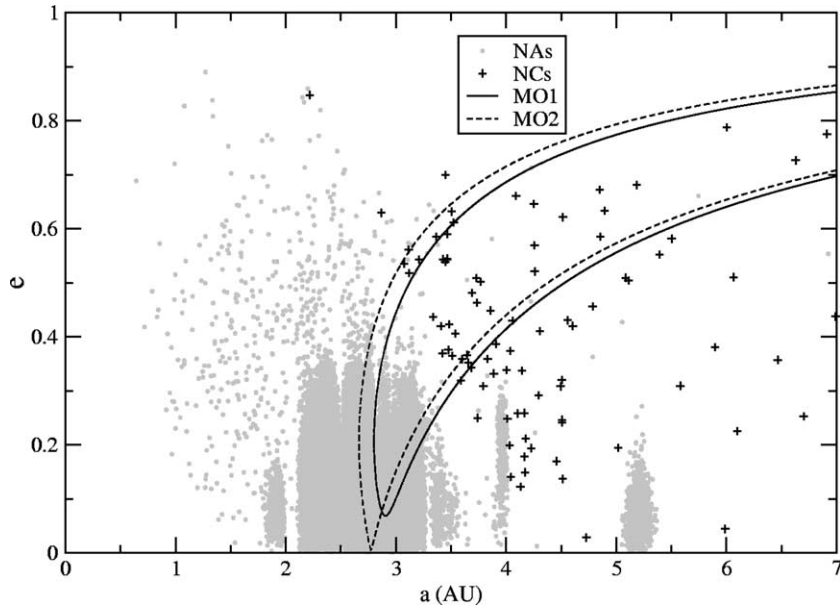


Fig. 3. Orbital solutions for the detected objects in the  $a, e$  plane (see text). The  $a$  axis has been terminated at 7 AU in order to better show the region of the Main Belt and Jupiter Trojans.

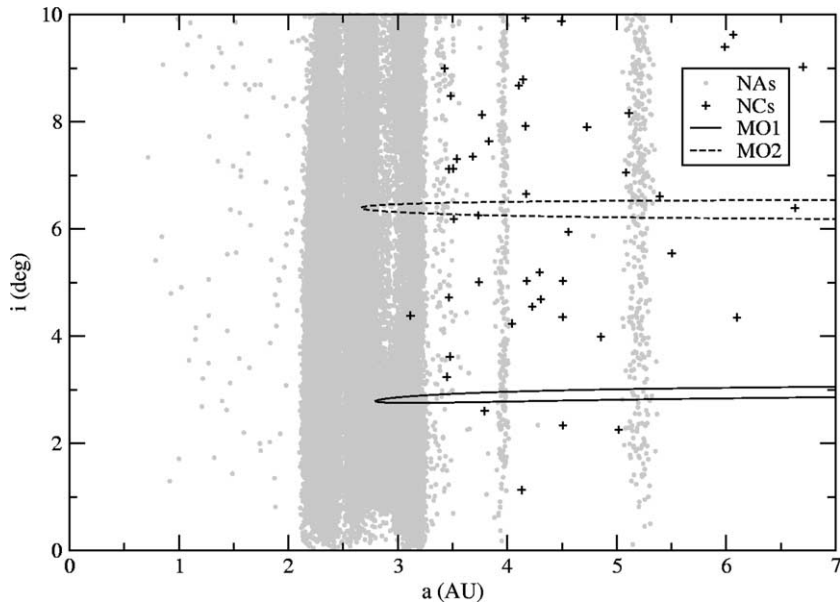


Fig. 4. Orbital solutions for the detected objects in the  $a, i$  plane (see text and Fig. 3).

ment region increases with time. Therefore, and to be useful for an actual recovery, this “window” has to be as narrow as possible. This is particularly important when dealing with HVSA. Indeed,

thanks to the knowledge of the geocentric distance  $d$ , we find that the admissible region becomes a *line* instead of an *area*, and consequently the triangulated ephemeris becomes a “linear” one. This

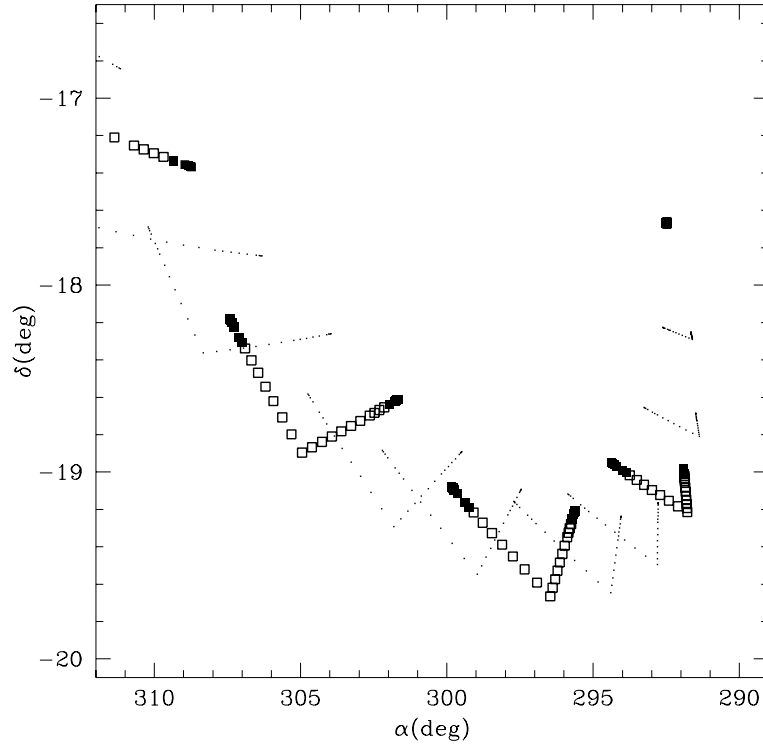


Fig. 5. Linear ephemeris for MO2. The plotted points span a 10 days interval, while squared symbols span a 30 days interval. The points (29 in total for each date) sample the solution of Figs. 3 and 4, where only  $a < 100$  AU have been considered. Open squares highlight solutions having  $a < 7$  AU (the most probable ones), while filled ones are for those having  $7 < a < 100$  AU. The single point on the upper right corner is the starting date for which all the solutions are coincident. The typical “V” shape of the distribution corresponds to the double solutions (see text) in Figs. 3 and 4, while the vertices correspond to solutions about  $e$  minimum. The linear regions follow each other in a clockwise direction reflecting mostly the Earth’s motion.

situation is illustrated in Fig. 5. This drastically reduces the number of frames required to sample the permitted area for the recovery of the objects. Fig. 5 shows that mapping the linear ephemeris would still require a reasonable number of frames (depending on the telescope used) even 2–3 months after the first detection.

### 3.4. Photometry

For each trail, aperture photometry is performed on every single image. Since the images were preprocessed (de-biased and flat-fielded) by the standard STScI pipeline, we directly summed the counts within 0.5 arcsec of each pixel in the trail. A local sky estimate was obtained in an adjacent area after the rejection of cosmic rays. The obtained digital counts were then put onto the

Vega System magnitude following the recipe in Holtzman et al. (1995), and in the particular case of ACS observations as in Bedin et al. (2004). Table 1 reports the derived magnitudes for MO1 and MO2, and allows us to address possible variations of their magnitude with time (possibly related to rotation). Given the errors (of the order of 0.04 and 0.07 magnitudes for MO1 and MO2) there is no clear indication of variability for MO1. On the other hand, the  $V_{606}$  magnitude of MO2 varies considerably, although, with only 3 exposures no firm conclusion can be reached.

MO1 has been detected in many frames, and most interestingly, in three different filters ( $V_{606}$ ,  $B_{475}$ ,  $I_{814}$ ). The color indices of MO1 may shed light on its nature. For this task, we computed the solar color indices in the same photometric system, that is  $B_{475}^{\odot} - V_{606}^{\odot} = 0.570$  and

Table 1  
Magnitudes of the two observed minor bodies

Filter	MO1	MO2
<i>B</i> <sub>475</sub> #1	20.46	
<i>B</i> <sub>475</sub> #2	20.41	
<i>B</i> <sub>475</sub> #3	20.30	
<i>B</i> <sub>475</sub> #4	20.34	
<i>B</i> <sub>475</sub> #5	20.34	
<i>V</i> <sub>606</sub> #1	19.78	22.38
<i>V</i> <sub>606</sub> #2	19.77	22.28
<i>V</i> <sub>606</sub> #3	19.76	22.00
<i>V</i> <sub>606</sub> #4	19.92	
<i>V</i> <sub>606</sub> #5	20.00	
<i>I</i> <sub>814</sub> #1	19.06	
<i>I</i> <sub>814</sub> #2	19.05	
<i>I</i> <sub>814</sub> #3	19.12	

$V_{606}^{\odot} - I_{814}^{\odot} = 0.569$ . The derived reflectivity (defined as  $R_i = 10^{-0.4((i-V_{606})_{MO} - (i-V_{606})_{\odot})}$ ) is:  $R_{475} = 1.03$ ,  $R_{606} = 1.00$  and  $R_{814} = 1.20$ . MO1's reflectivity indicates a red surface, a common property among outer MOs, like X-, M- D-type objects. Finally, assuming a geometric albedo of 0.1 in the *V*<sub>606</sub> filter, the estimated sizes of MO1 and MO2 are about 2.4 and 0.7 km, respectively. This further confirms the capability of *HST* to observe small objects.

#### 4. Conclusions

In this paper we report the identification of very short arcs (from 2 minor bodies) detected in *HST*

WFC/ACS images, and constrain the Keplerian elements of their orbits. Most interestingly, we address the problem of ephemeris prediction and show that in the particular case of HVSA's the confinement window for subsequent recovery of the MOs is significantly reduced to a *narrow linear region*, that would facilitate subsequent observations.

#### Acknowledgements

We thank the anonymous referee for interesting comments that helped to improve the layout of the paper. We also thank Prof. C. Barbieri for useful discussions and Dr. M. Clemens for a careful reading of the manuscript.

#### References

- Anderson, J., 2002. In: Arribas, S., Koekemoer, A., Whitmore, B. (Eds.), *HST Calibration Workshop 2002*. Baltimore: STScI, p. 13.
- Barbieri, C., Marchi, S., Migliorini, A., et al., 2004. Search for Minor Bodies with ASTROVIRTEL Archive Images. PSS, submitted.
- Bedin, L.R., Cassisi, S., Castelli, F., et al., 2004. MNRAS, submitted.
- Evans, R.W., Stapelfeldt, K.R., Peters, D.P., et al., 1998. *Icarus* 131, 261.
- Holtzman, J.A., Burrows, C.J., Casertano, S., et al., 1995. *PASP* 107, 1065.
- Milani, A., Gronchi, F.G., de' Micheli Vitturi, M., Knezevic, Z., 2004. Orbit Determination with Very Short Arcs. I Admissible Regions. CMDA, in press.